The effect of surge on riverine flood hazard and impact in deltas globally

Eilander, Dirk; Couasnon, Anaïs; Ikeuchi, Hiroaki; Muis, Sanne; Yamazaki, Dai; Winsemius, Hessel C.; Ward, Philip J.

DOI
10.1088/1748-9326/ab8ca6

Publication date
2020

Document Version
Final published version

Published in
Environmental Research Letters

Citation (APA)
Eilander, D., Couasnon, A., Ikeuchi, H., Muis, S., Yamazaki, D., Winsemius, H. C., & Ward, P. J. (2020). The effect of surge on riverine flood hazard and impact in deltas globally. *Environmental Research Letters*, *15*(10), 1-12. Article 104007. https://doi.org/10.1088/1748-9326/ab8ca6

The effect of surge on riverine flood hazard and impact in deltas globally

Environmental Research Letters

LETTER

The effect of surge on riverine flood hazard and impact in deltas globally

Dirk Eilander[1,2,6], Anaïs Couasnon[1], Hiroaki Ikeuchi[3], Sanne Muis[1,2], Dai Yamazaki[4], Hessel C Winsemius[2,5] and Philip J Ward[1]

[1] Institute for Environmental Studies (IVM), Vrije Universiteit Amsterdam, Amsterdam, The Netherlands
[2] Deltares, Delft, The Netherlands
[3] Ministry of Land, Infrastructure, Transport and Tourism, Kyoto, Japan
[4] Institute of Industrial Sciences, the University of Tokyo, Tokyo, Japan
[5] Delft University of Technology, Delft, The Netherlands
[6] Author to whom any correspondence should be addressed.

E-mail: dirk.eilander@vu.nl

Keywords: compound flooding, flood modelling, model coupling, flood hazard, flood impact

Supplementary material for this article is available online

OPEN ACCESS

RECEIVED
13 February 2020

REVISED
15 April 2020

ACCEPTED FOR PUBLICATION
23 April 2020

PUBLISHED
18 September 2020

Abstract

Current global riverine flood risk studies assume a constant mean sea level boundary. In reality high sea levels can propagate up a river, impede high river discharge, thus leading to elevated water levels. Riverine flood risk in deltas may therefore be underestimated. This paper presents the first global scale assessment of the joint influence of riverine and coastal drivers of flooding in deltas. We show that if storm surge is ignored, flood depths are significantly underestimated for 9.3% of the expected annual population exposed to riverine flooding. The assessment is based on extreme water levels at 3433 river mouth locations as modeled by a state-of-the-art global river routing model, forced with a multi-model runoff ensemble and bounded by dynamic sea level conditions derived from a global tide and surge reanalysis. We first classified the drivers of riverine flooding at each location into four classes: surge-dominant, discharge-dominant, compound-dominant or insignificant. We then developed a model experiment to quantify the effect of surge on flood hazard and impacts. Drivers of riverine flooding are compound-dominant at 19.7% of the locations analyzed, discharge-dominant at 69.2%, and surge-dominant at 7.8%. Compared to locations with either surge- or discharge-dominant flood drivers, locations with compound-dominant flood drivers generally have larger surge extremes and are located in basins with faster discharge response and/or flat topography. Globally, surge exacerbates 1-in-10 years flood levels at 64.0% of the locations analyzed, with a mean increase of 11 cm. While this increase is generally larger at locations with compound- or surge-dominant flood drivers, flood levels also increase at locations with discharge-dominant flood drivers. This study underlines the importance of including dynamic downstream sea level boundaries in (global) riverine flood risk studies.

1. Introduction

Currently, global flood risk studies either examine riverine or coastal floods (Jongman *et al* 2012, Hallegatte *et al* 2013, Hirabayashi *et al* 2013, Ward *et al* 2013, 2017, Hinkel *et al* 2014, Winsemius *et al* 2016, Vitousek *et al* 2017, Vousdoukas *et al* 2018, Dottori *et al* 2018). As such, these studies have not accounted for compound events, in which the combination of multiple drivers and/or hazards can interact to modulate risk (Zscheischler *et al* 2018). Compound flood events can occur from the interplay between riverine and coastal flood drivers, for instance when: high sea levels propagate up a river leading to elevated water levels; and/or the drainage of high river discharge is impeded by elevated sea levels. Current riverine flood hazard models ignore these interactions and potential dependencies between riverine and coastal flood drivers, which may result in an under- or overestimation of flood risk (Wahl *et al* 2015, Ward *et al* 2018). A first step towards accounting for compound events in global flood risk assessments is to understand where,

and under which conditions, compound events modulate flood hazard.

Several studies have addressed this by examining statistical dependence between different riverine and coastal flood drivers. They find dependence between: storm surge and precipitation in Australia (Zheng *et al* 2013, Wu *et al* 2017, 2018), the United States (Wahl *et al* 2015, Moftakhari *et al* 2017), Europe (Petroliagkis 2018, Bevacqua *et al* 2019), and the Netherlands (van den Hurk *et al* 2015, Ridder *et al* 2018); and storm surge and discharge in various parts of the United Kingdom (Svensson and Jones 2002, 2004, Lamb *et al* 2010, Hendry *et al* 2019), the Netherlands (Kew *et al* 2013, Klerk *et al* 2015, Khanal *et al* 2019), Texas (USA) (Couasnon *et al* 2018) and Italy (Bevacqua *et al* 2017). At the global scale significant dependence between storm surge and discharge based on observations was found at more than half of the locations studied (Ward *et al* 2018) and based on simulations at 26% of the locations studied (Couasnon *et al* 2020).

A limitation of dependence-based analyses of compound events is the need for event selection based on the flood drivers (e.g. surge or discharge) rather than flood levels. This introduces bias in the joint probability estimate, as events are either conditioned on one driver or on the other (Hawkes 2008, Zheng *et al* 2014). Furthermore, extreme water levels might be driven by events that are not extreme themselves (Serafin *et al* 2019). Van den Hurk *et al* (2015) were the first to carry out an impact-based analysis of compound events (i.e. based on the impact of compound flood drivers rather than their dependence) for a case study of a near-flood event in the Netherlands. An ensemble of surge and precipitation time-series were simulated with a regional climate model and used to force a hydrodynamic model of the inland water system. The simulated time-series were shuffled to remove dependence between surge and discharge. By comparing simulated water levels from original and 'shuffled' time-series, the effect of surge-precipitation dependence on extreme inland water levels was examined. However, analysis of compound events based on simulated flood levels rather than flood drivers requires models that realistically simulate interactions between multiple drivers.

At the global scale, the first river routing model to account for surge-discharge interactions was presented by Ikeuchi *et al* (2017). They included dynamic downstream sea level conditions in the global river routing model CaMa-Flood (Yamazaki *et al* 2011) by coupling it to the Global Tide and Surge Model (GTSM; Muis *et al* 2016). They show a significant difference in the annual maxima of riverine water levels between simulations using dynamic sea level boundary conditions and those using static mean sea levels. However, they did not assess the drivers of extreme water levels nor the effect of surge on flood levels specifically, leaving the question unanswered as to where, and to what extent, compound surge affects flooding.

To date, no global analysis of surge-discharge interactions based on simulated water levels exists. To fill this gap, we developed a global compound flood model framework with the aim to identify dominant flood drivers in deltas globally and assess the effect of surge on riverine flood hazard and impact. This is an important step towards including compound flood events in global flood risk modelling.

2. Methods

We developed a model framework consisting of a global river routing model forced by a multi-model ensemble of global hydrological models and bounded downstream by a global tide and surge model (section 2.1). We analyzed simulated water levels from the model framework to classify the dominant driver of riverine flooding in deltas globally (section 2.2); to assess the effect of surge on flood hazard (section 2.3); and flood impact in terms of population exposed (section 2.4).

2.1. Model framework

We developed a model framework for global compound flood simulations, see figure 1. We used a multi-model ensemble of runoff from tier 2 of the EartH2Observe (E2O) project (Dutra *et al* 2017, Schellekens *et al* 2017) with meteorological forcing from ERA-Interim (Dee *et al* 2011) and MSWEP v1.2 (Beck *et al* 2017), surge levels from the Global Tide and Surge Reanalysis (GTSR) based on the GTSM model (Muis *et al* 2016), and tide levels from the FES2012 model (Carrere *et al* 2012). These runoff and dynamic sea level (surge and tide) data were used to force the global hydrodynamic river routing model CaMa-Flood (Yamazaki *et al* 2011) to simulate riverine water levels and flood depths which are input for the analysis. Each model component is further discussed in this section.

We used CaMa-Flood version 3.6.4, which has a 1D routing scheme derived from HydroSHEDS (Lehner *et al* 2008). CaMa-Flood has an explicit representation of floodplains (Yamazaki *et al* 2011), which is crucial to correctly simulate discharge extremes (Zhao *et al* 2017). It solves the local inertial equation (Bates *et al* 2010, Yamazaki *et al* 2013), which accounts for backwater effects thereby enabling the simulation of riverine water levels bounded by dynamic sea level boundary conditions (Ikeuchi *et al* 2017). The CaMa-Flood schematization is based on unit-catchments at 15′ resolution, resulting in an average channel length of 29 km and average unit-catchment size of 529 km^2. The default Manning coefficient (s $m^{-1/3}$) is 0.03 for river channels and 0.10 for floodplains. The channel width is primarily based on the Global Width Database for Large Rivers (Yamazaki *et al* 2014). Similar to Ikeuchi *et al* (Ikeuchi

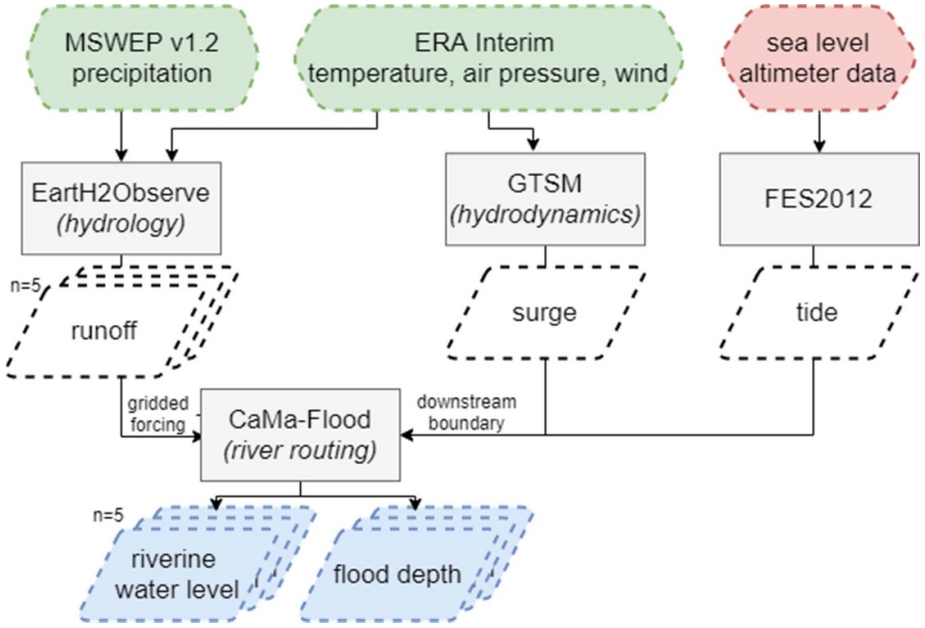

Figure 1. Model framework showing: the individual hydrologic and hydrodynamic models (grey); the meteorological forcing (green); tidal forcing (red); intermediate outputs (white); and final output used in our analysis (blue).

et al 2017), channel width W (m) for rivers smaller than 300 m and channel depth D (m) for all rivers are estimated as a function of simulated maximum 30 day upstream accumulated runoff R_{up} ($m^3\ s^{-1}$):

$$W = \max\left[0.40\ R_{up}^{0.75},\ 10.0\right] \quad (1)$$

$$D = \max\left[0.14\ R_{up}^{0.40},\ 2.0\right]. \quad (2)$$

We ran CaMa-flood for the period 1980–2014, with a spin-up period of two years using repeated forcing from the first year. Daily values of instantaneous discharge and water levels at 00:00 GTM are stored and used as input to the analysis in this study.

CaMa-Flood is forced by runoff, which is introduced at the head of each river channel section. The runoff data are obtained from the state-of-the-art global multi-model 15′ resolution ensemble dataset of E2O tier 2, which serves as a state of the art in current global hydrological modelling. The multi-model range in runoff stems from a combination of different total evaporation values and different storage dynamics in the models due to the different concepts and parameterization of runoff generation, see table 1, representing the uncertainty in land surface and hydrological processes (Schellekens *et al* 2017). For more details about the individual E2O models we refer the reader to Dutra *et al* (2017) and Schellekens *et al* (2017). From the available models we selected five that assume natural conditions, i.e. without anthropogenic water extractions. The runoff data were preprocessed to be on an identical grid from 90 North to 60 South, re-defined as a positive flux, and negative runoff values were set to zero in the JULES and ORCHIDEE data after discussions with the data owners (personal communication, 2018). Runoff data are then interpolated to the CaMa-Flood unit catchments using mass-conservative area-weighted averaging. We validated simulated discharge from CaMa-Flood forced by the E2O runoff ensemble against observations from the Global Runoff Data Centre with a focus on the magnitude and timing of discharge extremes. Although we find a large spread between individual models, the ensemble-mean performance statistics generally shows low model bias and small time lags compared to observations (see supplementary information (available online at stacks.iop.org/ERL/15/104007/mmedia)).

We introduced dynamic sea level boundary conditions from GTSM at the downstream end of each river in CaMa-Flood. GTSM is the first global hydrodynamic model to simulate surge levels, i.e. the response of the sea surface to changes in atmospheric pressure and wind speed (Pugh and Woodworth, Pugh *et al* 2014), with sufficiently high temporal and spatial resolution for this application (i.e. near-shore resolution of 2.5 km). It has good performance compared to tide gauge data and other models (Muis *et al* 2017, Wahl *et al* 2017, Cid *et al* 2018) and the timing and magnitude of storm surge peaks display sufficient performance for global scale compound flood analysis (Couasnon *et al* 2020). FES2012 simulates tides based on 32 tidal constituents and assimilation of satellite altimetry data (Carrere *et al* 2012) and is proven to have good near-shore performance (Stammer *et al* 2014). Mean sea level, tide, and surge are linearly superimposed to yield time-series of total still water levels at a 30-minute temporal resolution, thereby ignoring non-linear surge-tide interactions.

Table 1. E2O WRR2 multi-model ensemble of global hydrological models (GHMs) and land surface models (LSMs); based on Schellekens *et al* (2017) and Dutra *et al* (2017).

Model	Model type	Runoff process representation	Reference
HTESSEL	LSM	Saturation excess	(Balsamo *et al* 2009)
JULES	LSM	Saturation and infiltration excess	(Best *et al* 2011; Clark *et al* 2011)
LISFLOOD	GHM	Saturation and infiltration excess	(Van Der Knijff *et al* 2010)
ORCHIDEE	LSM	Green-Ampt infiltration	(Krinner *et al* 2005)
W3RA	GHM	Saturation and infiltration excess	(Van Dijk *et al* 2014)

A correction was applied to convert the vertical reference of still water levels from MSL to Earth Gravitational Model 1996 based on Mean Dynamic Topography data from Rio *et al* (2014), following Muis *et al* (2017). CaMa-Flood and GTSM do not have a perfectly joined interface: the most downstream river point in CaMa-Flood (hereafter referred to as river mouth) is often located inside the estuary, whereas GTSM output locations are slightly offshore. We therefore assumed a simplified estuary to schematize the missing link between the CaMa-Flood river mouth and GTSM. As the exact shape and bathymetry of estuaries globally is unknown, we extrapolated the channel width and depth from the CaMa-Flood river mouth, keeping the depth constant (Savenije 2005) and with a set length of 10 km. This estuary channel length is based on extensive validation by Ikeuchi *et al* (2017). River mouths in CaMa-Flood were coupled to the nearest GTSM output location within a maximum distance of 75 km. This distance threshold was selected as a trade-off between including as many river mouths as possible and excluding unrealistic links with GTSM output locations. Due to the relatively coarse resolution of the hydrological models, we focused on catchments with a minimum catchment size of 1000 km^2. Using these criteria, a downstream boundary was set for 3433 river mouths based on 2352 GTSM output locations.

2.2. Flood drivers

We classified the dominant drivers of flooding at each river mouth location, represented by annual maximum riverine water levels (h_{AM}) extracted from the simulated time series, into four classes: surge-dominant, discharge-dominant, compound-dominant or insignificant. The classification is based on the rank correlations between both h_{AM} and discharge and h_{AM} and skew surge (i.e. vertical difference between maximum still water level and high tide in a tidal cycle, stored as the maximum value at a daily time step). We used skew surge as it is the quantity of total water levels that might lead to flooding (Haigh *et al* 2016). Discharge and skew surge have a temporal resolution of 1 day and are selected as the maximum value within a 1-day window of the h_{AM} event to account for some delay between drivers and flood levels. Where both discharge and skew surge display a significant positive correlation ($p = 0.05$) with h_{AM} in a majority of the ensemble members, the flood drivers are classified as compound-dominant. Where either the discharge or the surge driver displays a significant positive correlation with h_{AM} in a majority of the ensemble members, flood drivers at this location are classified as discharge- or surge-dominant respectively. Locations where neither driver displays significant correlation in a majority of the ensemble members are classified as insignificant. The classification is illustrated for three contrasting locations in figure 2, where the drivers of flooding at the river mouths are classified as (a) surge-dominant, (b) discharge-dominant, (c) compound-dominant, or (d) insignificant. At the Mattepone River (c), large flood events (darker colors) are caused by either high skew surge or discharge or a combination of moderate skew surge and discharge. At the Dal (a) and Volta (b) rivers, large flood events are primarily caused by a single driver and extreme water levels can largely be explained using a univariate extreme value distribution. At the Xiaoling River (d) the return periods for h_{AM} do not result in perfect contours, possibly because drivers such as astronomical tide and waves are not included. This illustrates the relevance of studying compound events based on water levels rather than their individual drivers as shown before by e.g. Serafin *et al* (2019).

2.3. Flood levels

We developed three experiments, see table 2, to assess the difference in extreme riverine water levels with (scenario A) and without (scenario B) surge components included in the dynamic downstream sea level boundary. Surge levels were separated into a daily and seasonal component to assess their relative effects on flood levels. The seasonal component is associated with seasonal gyre circulation driven by synoptic pressure and wind differences at time scales longer than one month (e.g. Yang *et al* 1998, Palma *et al* 2004) and computed as monthly mean surge levels. The daily component is associated with surge due to short term meteorological variations in wind speed and sea level pressure and is computed as the difference between the total variation and seasonal component. In order to derive return periods of extreme water level beyond the length of our simulate time series, we fitted the 2-parameter Gumbel distribution using the L-moments method (Hosking and Wallis 2005). We find a difference in flood level to be significant if the sign of the

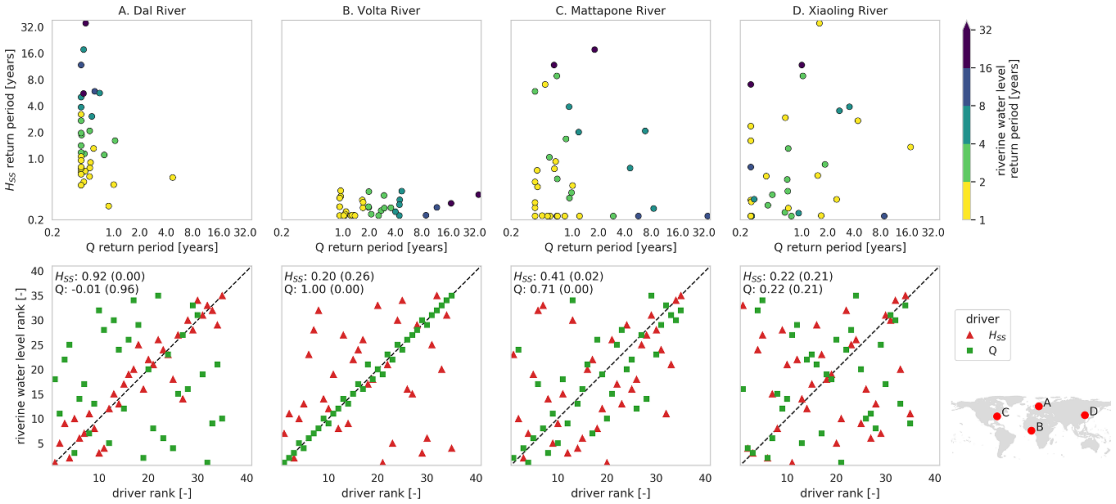

Figure 2. Classification of flood drivers illustrated for four contrasting locations based on the JULES model, a single ensemble-member, with (**top row**) the empirical return periods based on annual maxima riverine water level events h_{AM} as function of the empirical return period of its drivers skew surge (H_{SS}, *y*-axis) and discharge (Q, x-axis); and (**bottom row**) the Spearman rank correlation between h_{AM} events and H_{SS} (red triangles) and h_{AM} events and Q (green squares).

difference is the same for all ensemble members. Additionally, confidence intervals (5th–95th percentiles) are obtained from bootstrapping with a sample size of 1000, where the Gumbel parameters are bias-corrected for the mean of bootstrap parameter samples.

2.4. Population exposed

We analyzed the population exposed to flooding by overlaying downscaled inundation and population maps at 18" resolution, assuming no flood protection. The downscaled inundation maps are calculated based on the HydroSheds elevation (Lehner *et al* 2008). Cells are flooded when the flood depth of a unit-catchment is larger than the relative height above the outlet elevation of that unit-catchment. We used the 2010 WorldPop 30" resolution gridded population dataset (Tatem 2017) and resampled it to the resolution of the inundation depth maps using bi-linear interpolation, i.e. linear interpolation in *x* and *y* direction, of population density. We assume that if flood depth is larger than zero the total population in that grid cell is exposed. Flood depths are underestimated if surge is ignored in basins where we find a positive difference in simulated flood depths between a scenario with compared to a scenario without surge levels, see experiment 1 in table 2. We find flood depths to be significantly underestimated if the difference is positive for all ensemble members. Finally, we construct a risk curve based on the population exposed and flood exceedance probability at return periods ranging from 1 to 100 years. Expected annual population exposed is then calculated as the area under the risk curve using the trapezoidal rule (e.g. Ward *et al* 2011). Results of the ensemble-mean expected annual population exposed are presented.

3. Results and discussion

3.1. Flood drivers

Globally, flood drivers are classified as compound-dominant at 19.7% of the 3433 river mouth locations (figure 3(a)), with an average correlation of 0.57 between h_{AM} and skew surge and 0.63 between h_{AM} and discharge at these locations. Flooding is discharge-dominant at 69.2% of locations, with an average correlation of 0.84 between h_{AM} and discharge at these locations, and surge-dominant at 7.8% of locations, with an average correlation of 0.60 between h_{AM} and skew surge at these locations. The remaining 3.3% of locations are classified as insignificant as neither driver displays significant correlation in a majority of the ensemble members. Generally, compound flood drivers are found around large parts the USA, north-west Europe, the east coast of China, the east coast of Thailand and Malaysia, and around the Australian coastline. These regions are largely similar to those identified with high compound flood potential based on statistical dependence between simulated (Couasnon *et al* 2020) and observed (Ward *et al* 2018) surge and discharge. Notable differences occur along the east coast of the USA and the coast of the Baltic sea, likely due to the different selection criteria for compound events between the studies. For the UK we find a similar spatial pattern of locations with compound drivers compared to locations with a frequent joint occurrence of high skew surges and high river discharge (Hendry *et al* 2019), which are found more often along the west and south coasts relative to the east coast of the UK.

Next, we examined relationships between characteristics of river mouth locations and flood driver classification and examined whether these are

Table 2. Experiments to assess the effect of surge (components) on flood levels and impact based on the difference between the described scenarios.

	Dynamic downstream sea level boundary	
Experiment	Scenario A	Scenario B
1.Surge	Tide and surge levels	Tide
2.Seasonal surge component	Tide and seasonal surge levels	Tide
3.Daily surge component	Tide and daily surge levels	Tide and seasonal surge levels

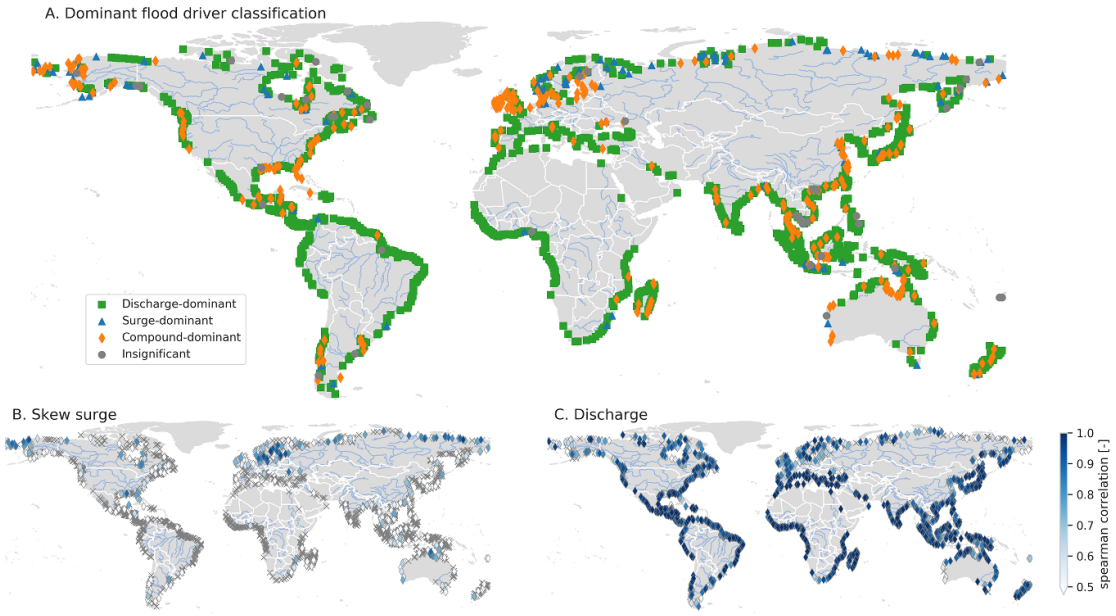

Figure 3. (a) Flood driver classification into four classes: surge-dominant (blue), discharge-dominant (green), compound-dominant (orange) or insignificant (grey) based on Spearman rank correlations between (b) riverine water level peaks and associated skew surge, and (c) riverine water level peaks and associated discharge where crosses indicate insignificant correlation. The largest 2000 out of 3433 rivers in terms of long-term average discharge, based on the complete simulated time series, are shown.

significantly different ($p = 0.01$) based on the Welch's t-test. Locations with surge- or compound-dominant drivers generally have higher annual maxima skew surge (figure 4(a)) and lower long-term average and annual maxima discharge (figures 4(c) and (e)) than locations with discharge-dominant drivers. While mean annual maxima skew surge levels are similar between locations with surge- and compound-dominant flood drivers, the inter-annual variability of skew surge (figure 4(b)) is generally larger for locations with compound-dominant flood drivers, indicating relatively large skew surge extremes at those locations. The high spatial heterogeneity of flood driver classification is likely due to different catchment characteristics. Generally, compound-dominant flood drivers occur in catchments with smaller area (although the difference is not significant) (figure 4(f)), shorter mean drainage length (figure 4(g)), and lower mean drainage slope, i.e. flatter topography (figure 4(h)). These results are in line with earlier results suggesting that compound events occur more frequently in smaller catchments with a faster response in the UK (Hendry *et al* 2019). In contrast to the results of Hendry *et al* (2019), we find that catchments with compound flood drivers have flatter instead of steeper topography. This could be explained by the selection of compound events: while Hendry *et al* (2019) focus on high surge and high discharge, we also sample events with high surge and moderate discharge. Under these conditions, surge is more likely to propagate up rivers with flat topography.

3.2. Flood levels

Our results show that 1-in-10 years (T10) flood levels are generally exacerbated due to surge, with an overall ensemble-mean difference in riverine water level at the river mouth ($\overline{\Delta h}$) of 11 cm between Scenario A and B of experiment 1 in table 2. $\overline{\Delta h}$ is significant and positive at 64.0% of the 3433 river mouth locations studied, and significant and negative at 12.2%, while at 23.9% the ensemble members do not agree on the sign of $\overline{\Delta h}$, and are therefore classified as insignificant (figure 5(a)). Moreover, $\overline{\Delta h}$ is larger than the 5%–95% bootstrap confidence intervals for all ensemble members at 17.3% of the locations. $\overline{\Delta h}$ is largest at locations with surge-dominant (28 cm) or

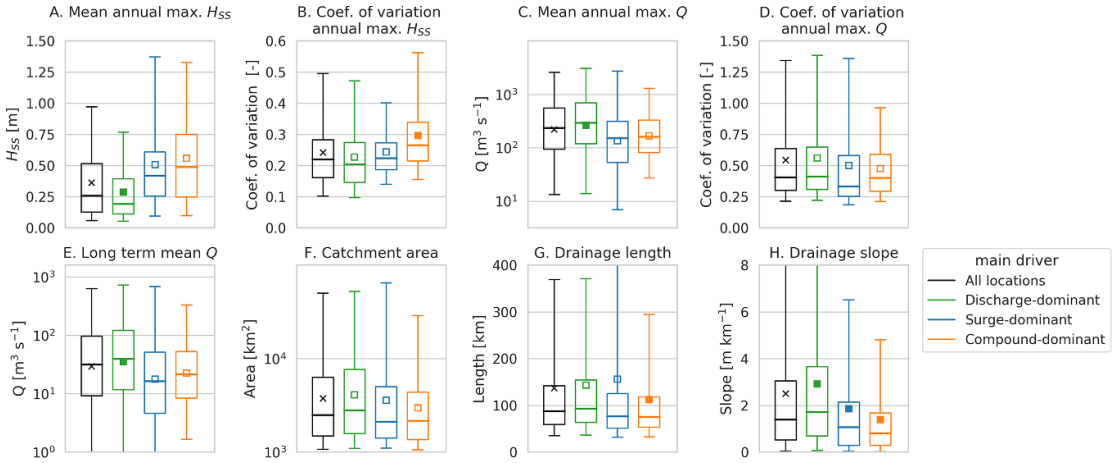

Figure 4. Box-whisker plots showing distributions of offshore and basin characteristics for all river mouth location and for different classes of flood drivers: discharge-dominant (green), surge-dominant (blue) or compound-dominant (orange); the overall distribution is shown in black. The characteristics are: (a) the mean and (b) coefficient of variation of annual maxima skew surge (H_{SS}); (c) mean and (d) coefficient of variation of annual maxima discharge (Q); (e) long term mean Q; (f) catchment area; (g) mean drainage path length; and (f) mean drainage path slope. The boxes show the interquartile range (25th–75th percentile), the thick line the median, the whiskers the 5th−95th percentiles, and the markers the mean. The markers are filled if significantly different ($p = 0.01$) from other driver classes based on the Welch's t-test.

compound-dominant flood drivers (30 cm), while $\overline{\Delta h}$ is small (3 cm) at locations with discharge-dominant flood drivers. Generally speaking, regions with the largest positive $\overline{\Delta h}$ are the coasts of Alaska (US), North-West Europe, the Chinese coast at the Yellow Sea, and the coast on the Gulf of Carpentaria (Australia), which are all characterized by large surge extremes. Generally, at higher return periods the number of locations with significant $\overline{\Delta h}$ decreases, while the overall $\overline{\Delta h}$ at locations with a significant difference increases, see table 3. To better understand $\overline{\Delta h}$, we separate it into a difference in riverine water level due to a seasonal ($\overline{\Delta h}_{seasonal}$, see experiment 2 in table 2) and daily component ($\overline{\Delta h}_{daily}$, see experiment 3 in table 2). The daily component is mainly associated with surge due to short term meteorological variations in wind speed and sea level pressure, while the seasonal component is associated with seasonal gyre circulation (e.g. Yang *et al* 1998, Palma *et al* 2004). Large positive values of $\overline{\Delta h}$ are mainly caused by $\overline{\Delta h}_{daily}$, which for T10 is positive at 73.1% of the locations with a mean increase of 14 cm (figure 5(b)). Negative $\overline{\Delta h}$ is mainly caused by $\overline{\Delta h}_{seasonal}$, negative at 50.3% of the locations, with a mean decrease of 3 cm (figure 5(c)). In some areas, $\overline{\Delta h}_{seasonal}$ and $\overline{\Delta h}_{daily}$ are both positive and combine to a larger positive $\overline{\Delta h}$; examples are most of the South and East coasts of Asia and North coast of Australia where the positive seasonal effects coincide with the main storm season. For North Australia this is during the Australian-Indonesian monsoon in the local summer months (DJF), which causes high seasonal surge levels (Haigh *et al* 2013a) and is also known to be the season with strong tropical cyclone activity (Haigh *et al* 2013b). This results in strong dependence between surge and precipitation (Wu *et al* 2018). In other areas, a positive $\overline{\Delta h}_{daily}$ is alleviated by a negative $\overline{\Delta h}_{seasonal}$; examples are the coastline of the Hudson Bay (Canada), the Argentinian coast, and the South coasts of Australia. At the Argentinian coast, negative $\overline{\Delta h}_{seasonal}$ is caused by offshore wind stress throughout the year (Palma *et al* 2004) while positive $\overline{\Delta h}_{daily}$ is caused by large storm surge events, especially around Mar del Plata (Fiore *et al* 2009). Compared to Ikeuchi *et al* (2017). who reported on the effect of total sea level variations on riverine water levels, we find similar areas with large $\overline{\Delta h}$. Notable differences between the two studies include the Gulf of Carpentaria and North Sea coast, where we find larger $\overline{\Delta h}$, which can be attributed to relatively high surge levels.

3.3. Population exposed

If surge is ignored, flood depths (and thus flood risk) are significantly underestimated for 30.7 million out of 332.0 million of the total expected annual population exposed (ensemble-mean), i.e. 9.3%. In absolute numbers, most people for whom flood depths are underestimated live along the densely populated coasts of east and south Asia. In relative numbers, flood depths are underestimated for a large percentage of the total expected annual population exposed (ensemble-mean) in small coastal basins with compound- or surge-dominant drivers, but also larger basins along the Hudson Bay coastline (Canada), the Neva (Russia), and the Elbe and Weser (Germany), see figure 6.

3.4. Limitations of the datasets and methods

The magnitude and timing of annual maxima surge and discharge estimates from GTSM and CaMa-Flood are not perfectly resolved, see section 2.2. To account for some of these uncertainties, we used the

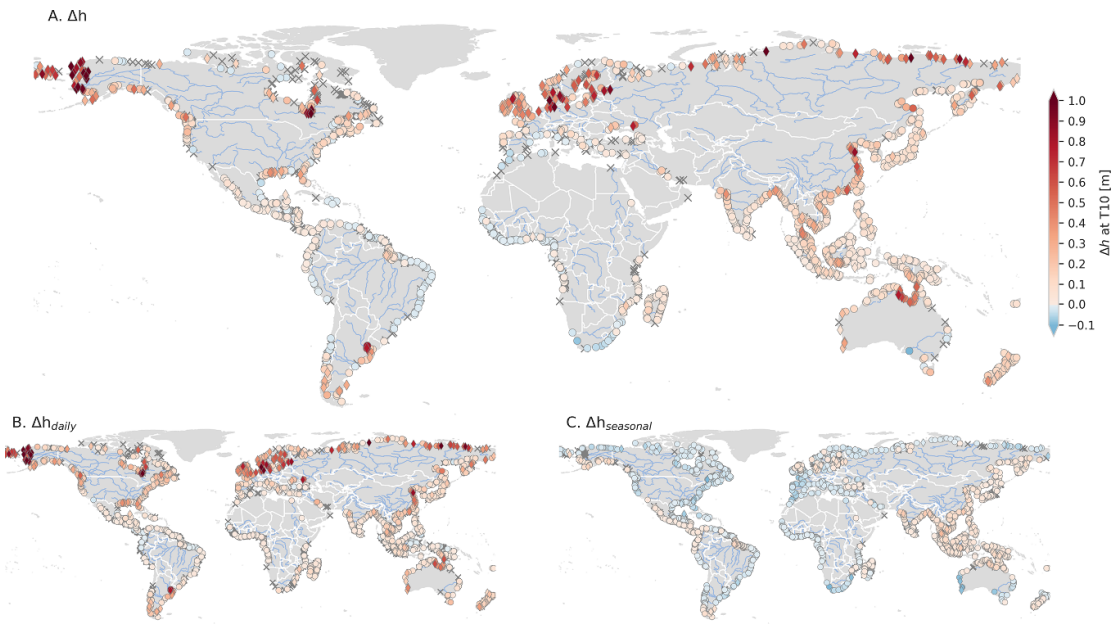

Figure 5. Ensemble-mean difference in 1-in-10 years flood levels at the river mouth due to (a) surge; separated into (b) a daily and (c) a seasonal component. At locations indicated with a diamond, the difference is larger than the 5%–95% bootstrap confidence intervals for all ensemble members; at locations indicated with a cross, the sign of difference is not consistent across the ensemble members. The largest 2000 out of 3433 rivers in terms of long-term average discharge, based on the complete simulated time series are shown.

Table 3. Percentage of 3433 river mouth locations with an insignificant, positive significant, or negative significant ensemble-mean difference in flood level due to surge. The overall ensemble-mean difference ($\overline{\Delta h}$) is given between parenthesis.

Return period (years)	2	10	50	100
Insignificant	17.9%	23.9%	36.0%	39.6%
Significant and positive	66.2% (12 cm)	64.0% (16 cm)	56.1% (22 cm)	53.6% (24 cm)
Significant and negative	15.8% (−2 cm)	12.2% (−2 cm)	8.0% (−2 cm)	6.8% (−3 cm)

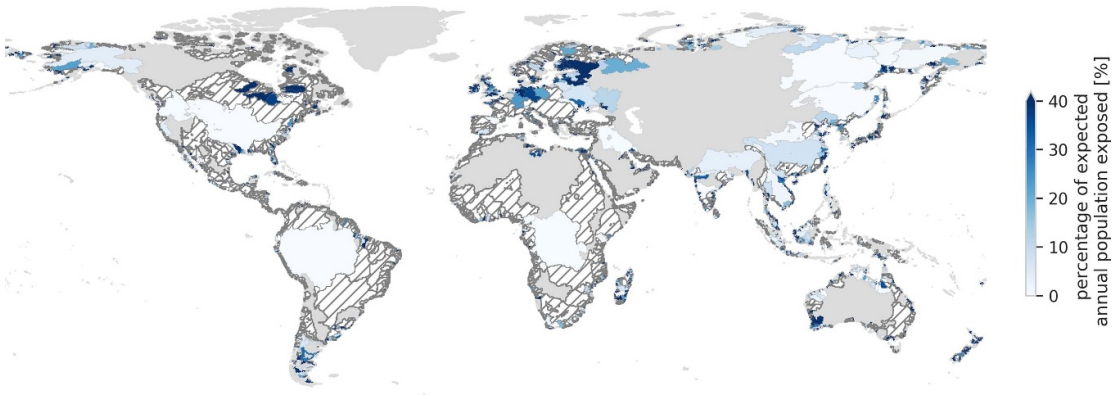

Figure 6. Percentage of ensemble-mean expected annual mean population exposed to riverine flooding for whom flood depths are underestimated if surge is ignored, assuming no flood protection. Hatched basins show insignificant difference in flood depth; grey areas are not simulated (i.e. Greenland and Iceland) or not connected with GTSM (e.g. Irrawaddy). Note that the entire basins are colored while the underestimation of flood depths occurs in the coastal areas of the basin.

E2O tier 2 multi-model ensemble. We only used a single surge model as there is less uncertainty in the timing of surge compared to discharge simulations (Couasnon *et al* 2020) and to date there is only one global hydrodynamic surge model with sufficient temporal and spatial resolution for this application.

Some processes that could affect the classification of flood drivers are currently missing in the model framework. GTSM does not account for non-linear surge-tide interactions, or inter-annual variability in mean sea levels due to steric effects or waves, which can be important drivers of coastal flooding

at regional scales (e.g. Arns *et al* 2017, Vitousek *et al* 2017, Muis *et al* 2018). CaMa-Flood does not take the operation of reservoirs into account, while these will significantly change the magnitude and timing of discharge peaks (Mateo *et al* 2014, Fleischmann *et al* 2019). Local variations in bathymetry that are not addressed in the CaMa-Flood and/or GTSM models may cause bias in the absolute water levels locally. Near-shore and estuarine areas are still very difficult to resolve accurately in global bathymetry datasets (Weatherall *et al* 2015) and therefore provide large uncertainty for global compound flood risk analysis. The model framework does not account for the influence of discharge on local sea levels as these are derived independently. A two-way coupling between GTSM and CaMa-Flood would be required to assess the complete interactions.

Furthermore, we did not account for uncertainties in the meteorological forcing. While the MSWEP V1.2 precipitation dataset is known to have a good performance compared to many other state-of-the-art global precipitation datasets, it has some caveats, including spurious drizzle and attenuated peaks (Beck *et al* 2017). GTSM is known to underestimate surge in areas with tropical cyclones due to the coarse spatial resolution of ERA-Interim (Muis *et al* 2016, Dullaart *et al* 2020). This might lead to an underestimation of the contribution of surge to riverine flooding in areas with high cyclone activity. The classification of flood drivers is less sensitive to this underestimation as it is based on the relative rank of the flood drivers. Only if different annual maximum flood events are selected as a result of this underestimation, it may affect the classification. In general, recent updates of meteorological forcing datasets providing higher resolution data and/or longer timeseries, including MSWEP v2 (Beck *et al* 2018) and ERA5 (the successor to ERA-Interim), could further improve the robustness of our results.

We estimated riverine flood extent and subsequent flood impact based on downscaled flood depths from CaMa-Flood. To focus on the effect of surge on flood impact we assumed no flood protection as accurate global data on protection standards are sparse (Scussolini *et al* 2016) while simulated flood impacts very sensitive to flood protection (Ward *et al* 2013). Furthermore, direct coastal or pluvial flooding could further influence the simulated water levels. To resolve complex hydrodynamic interactions between different flood drivers in coastal areas, higher resolution 2D flood models are required. A nested modelling approach (e.g. Hoch *et al* 2019) could be a possible avenue to explore in order to take a more integrate approach to improve flood modelling in coastal areas without compromising too much on computationally efficiency.

4. Conclusions and future work

In this study we present the first mapping of the dominant drivers of riverine flooding in deltas globally and assessed the effect of surge on riverine flood hazard and impact. The research highlights the importance of including dynamic sea level boundary conditions in riverine flood risk models. Drivers of riverine flooding are compound-dominant at 19.7% of the locations analyzed, discharge-dominant at 69.2% and surge-dominant at 7.8%. Compared to locations with either surge- or discharge-dominant flood drivers, locations with compound-dominant flood drivers generally have larger surge extremes and are in basins with faster discharge response and/or flat topography. Globally, surge exacerbates T10 flood levels at 64.0% of the locations analyzed, with a mean increase of 11 cm. While this increase is the largest at locations with compound- or surge-dominant flood drivers, surge also affects flood levels at locations with discharge-dominant flood drivers. A small decrease in T10 flood levels is observed at 12.2% of locations analyzed due to negative surge levels associated with dominant seasonal gyre circulations. Finally, we show that if surge is ignored, flood depths are underestimated for 30.7 million out of a total of 332.0 million (9.3%) expected annual population exposed (ensemble-mean).

In general, large scale flood risk studies would improve from a more holistic representation of flooding in our models, including direct coastal flooding from storm surges and waves as well as pluvial and fluvial flooding. This may require more detailed 2D hydrodynamic modelling in coastal areas to resolve complex hydrodynamic interactions between these different drivers. While we focused on classifying the drivers of riverine flooding per location, investigating the drivers and meteorological conditions of individual flood events would further enhance our understanding of compound events.

Data Availability

The data that support the findings of this study are openly available. The source code for the simulation, pre- and postprocessing and the analysis is available on GitHub at https://github.com/DirkEilander/compound_hotspots (DOI: 10.5281/zenodo.3665811). The dataset of simulated water levels and discharge at 3433 river mouth locations globally, including several components of nearshore still water levels is available on Zenodo (DOI: 10.5281/zenodo.3665734).

Acknowledgments

The research leading to these results received funding from the Netherlands Organisation for Scientific

Research (NWO) in the form of a VIDI grant (Grant No. 016.161.324) and the TOUGOU program by MEXT Japan (JPMXD0717935457), and JSPS KAKENHI (Grant No. JP16J07523).

Competing Financial Interest Statement

The authors declare no competing financial interests.

ORCID iDs

Dirk Eilander https://orcid.org/0000-0002-0951-8418
Anaïs Couasnon https://orcid.org/0000-0001-9372-841X
Hiroaki Ikeuchi https://orcid.org/0000-0002-4824-0594
Sanne Muis https://orcid.org/0000-0002-8145-0171
Dai Yamazaki https://orcid.org/0000-0002-6478-1841
Hessel C Winsemius https://orcid.org/0000-0001-5471-172X
Philip J Ward https://orcid.org/0000-0001-7702-7859

References

Arns A, Dangendorf S, Jensen J, Talke S, Bender J and Pattiaratchi C 2017 Sea-level rise induced amplification of coastal protection design heights *Sci. Rep.* **7** 40171

Balsamo G, Beljaars A, Scipal K, Viterbo P, van den Hurk B J J M, Hirschi M and Betts A K 2009 A revised hydrology for the ECMWF model: verification from field site to terrestrial water storage and impact in the integrated forecast system *J. Hydrometeorol.* **10** 623–43

Bates P D, Horritt M S and Fewtrell T J 2010 A simple inertial formulation of the shallow water equations for efficient two-dimensional flood inundation modelling *J. Hydrol.* **387** 33–45

Best M J *et al* 2011 The Joint UK Land Environment Simulator (JULES), model description – part 1: energy and water fluxes *Geosci. Model Dev.* **4** 677–99

Beck H E, Van Dijk A I J M, Levizzani V, Schellekens J, Miralles D G, Martens B and De Roo A P J 2017 MSWEP: 3-hourly 0.25 deg; global gridded precipitation (1979–2015) by merging gauge, satellite, and reanalysis data *Hydrol. Earth Syst. Sci.* **21** 589–615

Beck H E, Wood E F, Pan M, Fisher C K, Miralles D G, van Dijk A I J M, Mcvicar T R and Adler R F 2018 MSWEP V2 global 3-hourly 0.1° precipitation: methodology and quantitative assessment *Bull. Am. Meteorol. Soc.* **100** 473–500

Bevacqua E, Maraun D, Hobæk Haff I, Widmann M and Vrac M 2017 Multivariate statistical modelling of compound events via pair-copula constructions: analysis of floods in Ravenna (Italy) *Hydrol. Earth Syst. Sci.* **21** 2701–23

Bevacqua E, Maraun D, Vousdoukas M I, Voukouvalas E, Vrac M, Mentaschi L and Widmann M 2019 Higher probability of compound flooding from precipitation and storm surge in Europe under anthropogenic climate change *Sci. Adv.* **5** eaaw5531

Carrere L, Lyard F, Cancet M, Guillot A and Roblou L 2012 FES2012: A new global tidal model taking advantage of nearly 20 years of altimetry *20 Years of Progress in Radar Altimatry (Venice, Italy, 24–29 September 2013)* p 6

Cid A, Wahl T, Chambers D P and Muis S 2018 Storm surge reconstruction and return water level estimation in southeast Asia for the 20th century *J. Geophys. Res. Ocean.* **123** 437–51

Clark D B *et al* 2011 The Joint UK Land Environment Simulator (JULES), model description – part 2: carbon fluxes and vegetation dynamics *Geosci. Model Dev.* **4** 701–22

Couasnon A, Eilander D, Muis S, Veldkamp T I E, Haigh I D, Wahl T, Winsemius H C and Ward P J 2020 Measuring compound flood potential from river discharge and storm surge extremes at the global scale *Nat. Hazards Earth Syst. Sci.* **20** 489–504

Couasnon A, Sebastian A and Morales-Nápoles O 2018 A copula-based Bayesian network for modeling compound flood hazard from riverine and coastal interactions at the catchment scale: an application to the Houston Ship Channel *Texas Water* **10** 1190

Dee D P *et al* 2011 The ERA-Interim reanalysis: configuration and performance of the data assimilation system *Q. J. R. Meteorol. Soc.* **137** 553–97

Dottori F *et al* 2018 Increased human and economic losses from river flooding with anthropogenic warming *Nat. Clim. Chang.* **8** 781–6

Dullaart J C M, Muis S, Bloemendaal N and Aerts J C J H 2020 Advancing global storm surge modelling using the new ERA5 climate reanalysis *Clim. Dyn.* **54** 1007–21

Dutra E *et al* 2017 *Report on the improved Water Resources Reanalysis*

Fiore M M E, D'Onofrio E E, Pousa J L, Schnack E J and Bértola G R 2009 Storm surges and coastal impacts at Mar del Plata, Argentina *Cont. Shelf Res.* **29** 1643–9

Fleischmann A, Collischonn W, Paiva R and Tucci C E 2019 Modeling the role of reservoirs versus floodplains on large-scale river hydrodynamics *Nat. Hazards* **99** 1075–104

Haigh I D, Macpherson L R, Mason M S, Wijeratne E M S, Pattiaratchi C B, Crompton R P and George S 2013a Estimating present day extreme water level exceedance probabilities around the coastline of Australia: tropical cyclone-induced storm surges *Clim. Dyn.* **42** 139–57

Haigh I D, Wadey M P, Wahl T, Ozsoy O, Nicholls R J, Brown J M, Horsburgh K and Gouldby B 2016 Spatial and temporal analysis of extreme sea level and storm surge events around the coastline of the UK *Sci. Data* **3** 160107

Haigh I D, Wijeratne E M S S, Macpherson L R, Pattiaratchi C B, Mason M S, Crompton R P and George S 2013b Estimating present day extreme water level exceedance probabilities around the coastline of Australia: tides, extra-tropical storm surges and mean sea level *Clim. Dyn.* **42** 121–38

Hallegatte S S, Green C, Nicholls R J and Corfee-Morlot J 2013 Future flood losses in major coastal cities *Nat. Clim. Chang.* **3** 802–6

Hawkes P J 2008 Joint probability analysis for estimation of extremes *J. Hydraul. Res.* **46** 246–56

Hendry A, Haigh I D, Nicholls R J, Winter H, Neal R, Wahl T, Joly-Laugel A and Darby S E 2019 Assessing the characteristics and drivers of compound flooding events around the UK coast *Hydrol. Earth Syst. Sci.* **23** 3117–39

Hinkel J, Lincke D, Vafeidis A T, Perrette M, Nicholls R J, Tol R S J, Marzeion B, Fettweis X, Ionescu C and Levermann A 2014 Coastal flood damage and adaptation costs under 21st century sea-level rise *Proc. Natl. Acad. Sci.* **111** 3292–7

Hirabayashi Y, Mahendran R, Koirala S, Konoshima L, Yamazaki D, Watanabe S, Kim H and Kanae S 2013 Global flood risk under climate change *Nat. Clim. Chang.* **3** 816–21

Hoch J M, Eilander D, Ikeuchi H, Baart F and Winsemius H C 2019 Evaluating the impact of model complexity on flood wave propagation and inundation extent with a hydrologic-hydrodynamic model coupling framework *Nat. Hazards Earth Syst. Sci.* **19** 1723–35

Hosking J R M and Wallis J R 2005 *Regional Frequency Analysis: An Approach Based on L-moments* (Cambridge: Cambridge University Press)

Ikeuchi H, Hirabayashi Y, Yamazaki D, Muis S, Ward P J, Winsemius H C, Verlaan M and Kanae S 2017 Compound simulation of fluvial floods and storm surges in a global coupled river-coast flood model: model development and its application to 2007 cyclone sidr in Bangladesh *J. Adv. Model. Earth Syst.* **9** 1–32

Jongman B, Ward P J and Aerts J C J H 2012 Global exposure to river and coastal flooding: long term trends and changes *Glob. Environ. Chang.* **22** 823–35

Kew S F, Selten F M, Lenderink G and Hazeleger W 2013 The simultaneous occurrence of surge and discharge extremes for the Rhine delta *Nat. Hazards Earth Syst. Sci.* **13** 2017–29

Khanal S, Ridder N, Vries H D, Terink W and Hurk B V D 2019 Storm surge and extreme river discharge: a compound event analysis using ensemble impact modeling *Front. Earth Sci.* **7** 1–15

Klerk W J, Winsemius H C, van Verseveld W J, Bakker A M R and Diermanse F L M 2015 The co-incidence of storm surges and extreme discharges within the Rhine–Meuse Delta *Environ. Res. Lett.* **10** 035005

Krinner G, Viovy N, de Noblet-Ducoudré N, Ogée J, Polcher J, Friedlingstein P, Ciais P, Sitch S and Prentice I C 2005 A dynamic global vegetation model for studies of the coupled atmosphere-biosphere system *Global Biogeochem. Cycles* **19** GB1015

Lamb R, Keef C, Tawn J, Laeger S, Meadowcroft I, Surendran S, Dunning P and Batstone C 2010 A new method to assess the risk of local and widespread flooding on rivers and coasts *J. Flood Risk Manag.* **3** 323–36

Lehner B, Verdin K and Jarvis A 2008 New global hydrography derived from spaceborne Elevation data Eos *Trans. Am. Geophys. Union* **89** 93

Mateo C M, Hanasaki N, Komori D, Tanaka K, Kiguchi M, Champathong A, Sukhapunnaphan T, Yamazaki D and Oki T 2014 Assessing the impacts of reservoir operation to floodplain inundation by combining hydrological, reservoir management, and hydrodynamic models Water *Resour. Res.* **50** 7245–66

Moftakhari H R, Salvadori G, Aghakouchak A, Sanders B F and Matthew R A 2017 Compounding effects of sea level rise and fluvial flooding *Proc. Natl. Acad. Sci.* **114** 9785–90

Muis S, Haigh I D, Guimarães Nobre G, Aerts J C J H and Ward P J 2018 Influence of El Niño-Southern Oscillation on global coastal flooding *Earth's Futur* **6** 1311–22

Muis S, Verlaan M, Nicholls R J, Brown S, Hinkel J, Lincke D, Vafeidis A T, Scussolini P, Winsemius H C and Ward P J 2017 A comparison of two global datasets of extreme sea levels and resulting flood exposure *Earth's Futur* **5** 379–92

Muis S, Verlaan M, Winsemius H C, Aerts J C J H and Ward P J 2016 A global reanalysis of storm surges and extreme sea levels *Nat. Commun.* **7** 11969

Palma E D, Matano R P and Piola A R 2004 A numerical study of the Southwestern Atlantic Shelf circulation: barotropic response to tidal and wind forcing *J. Geophys. Res. Ocean.* **109**

Petroliagkis T I 2018 Estimations of statistical dependence as joint return period modulator of compound events - Part 1: storm surge and wave height *Nat. Hazards Earth Syst. Sci.* **18** 1937–55

Pugh D and Woodworth P 2014 Tidal analysis and prediction *Sea-Level Science* (Cambridge: Cambridge University Press) pp 60–96

Ridder N, de Vries H and Drijfhout S 2018 The role of atmospheric rivers in compound events consisting of heavy precipitation and high storm surges along the Dutch coast *Nat. Hazards Earth Syst. Sci.* **18** 3311–26

Rio M-H, Mulet S and Picot N 2014 Beyond GOCE for the ocean circulation estimate: synergetic use of altimetry, gravimetry, and in situ data provides new insight into geostrophic and Ekman currents *Geophys. Res. Lett.* **41** 8918–25

Savenije H H G 2005 Tide and Estuary Shape *Salinity and Tides in Alluvial Estuaries*, ed H H G Savenije (Amsterdam: Elsevier) pp 23–68

Schellekens J *et al* 2017 A global water resources ensemble of hydrological models: the eartH2Observe Tier-1 dataset *Earth Syst. Sci. Data* **9** 389–413

Scussolini P, Aerts J C J H, Jongman B, Bouwer L M, Winsemius H C, de Moel H and Ward P J 2016 FLOPROS: an evolving global database of flood protection standards *Nat. Hazards Earth Syst. Sci.* **16** 1049–61

Serafin K A, Ruggiero P, Parker K and Hill D 2019 What's streamflow got to do with it? A probabilistic simulation of the competing oceanographic and fluvial processes driving along-river extreme water levels *Nat. Hazards Earth Syst. Sci.* **19** 1415–31

Stammer D *et al* 2014 Accuracy assessment of global barotropic ocean tide models *Rev. Geophys.* **52** 243–82

Svensson C and Jones D A 2002 Dependence between extreme sea surge, river flow and precipitation in eastern *Britain Int. J. Climatol.* **22** 1149–68

Svensson C and Jones D A 2004 Dependence between sea surge, river flow and precipitation in south and west *Britain Hydrol. Earth Syst. Sci.* **8** 973–92

Tatem A J 2017 WorldPop, open data for spatial demography *Sci. Data* **4**

van den Hurk B J J M, van Meijgaard E, De Valk P, van Heeringen K-J J and Gooijer J 2015 Analysis of a compounding surge and precipitation event in the Netherlands *Environ. Res. Lett.* **10** 035001

Van Der Knijff J M, Younis J and De Roo A P J 2010 LISFLOOD: a GIS-based distributed model for river basin scale water balance and flood simulation *Int. J. Geogr. Inf. Sci.* **24** 189–212

van Dijk A I J M, Renzullo L J, Wada Y and Tregoning P 2014 A global water cycle reanalysis (2003-2012) merging satellite gravimetry and altimetry observations with a hydrological multi-model ensemble *Hydrol. Earth Syst. Sci.* **18** 2955–73

Vitousek S, Barnard P L, Fletcher C H, Frazer N, Erikson L and Storlazzi C D 2017 Doubling of coastal flooding frequency within decades due to sea-level rise *Sci. Rep.* **7** 1399

Vousdoukas M I, Mentaschi L, Voukouvalas E, Bianchi A, Dottori F and Feyen L 2018 Climatic and socioeconomic controls of future coastal flood risk in Europe *Nat. Clim. Chang.* **8**

Wahl T, Haigh I D, Nicholls R J, Arns A, Dangendorf S, Hinkel J and Slangen A B A 2017 Understanding extreme sea levels for broad-scale coastal impact and adaptation analysis *Nat. Commun.* **8** 1–12

Wahl T, Jain S, Bender J, Meyers S D and Luther M E 2015 Increasing risk of compound flooding from storm surge and rainfall for major US cities *Nat. Clim. Chang.* **5** 1–6

Ward P J, Couasnon A, Eilander D, Haigh I D, Hendry A, Muis S, Veldkamp T I E, Winsemius H C and Wahl T 2018 Dependence between high sea-level and high river discharge increases flood hazard in global deltas and estuaries *Environ. Res. Lett.* **13** 084012

Ward P J, Jongman B, Sperna Weiland F C, Bouwman A, van Beek R L P H, Bierkens M F P P, Ligtvoet W and Winsemius H C 2013 Assessing flood risk at the global scale: model setup, results, and sensitivity *Environ. Res. Lett.* **8** 44019

Ward P J *et al* 2017 A global framework for future costs and benefits of river-flood protection in urban areas *Nat. Clim. Chang.* **7** 642–6

Ward P J de Moel H and Aerts J C J H 2011 How are flood risk estimates affected by the choice of return-periods? *Nat. Hazards Earth Syst. Sci.* **11** 3181–95

Weatherall P, Marks K M, Jakobsson M, Schmitt T, Tani S, Arndt J E, Rovere M, Chayes D, Ferrini V and Wigley R 2015 A new digital bathymetric model of the world's oceans *Earth Sp. Sci.* **2** 331–45

Winsemius H C et al 2016 Global drivers of future river flood risk *Nat. Clim. Chang.* **6** 381–5
Wu W, Mcinnes K, O'grady J, Hoeke R, Leonard M and Westra S 2018 Mapping dependence between extreme rainfall and storm surge *J. Geophys. Res. Ocean.* **123** 2461–74
Wu W, Westra S and Leonard M 2017 A basis function approach for exploring the seasonal and spatial features of storm surge events *Geophys. Res. Lett.* **44** 7356–65
Yamazaki D, de Almeida G A M and Bates P D 2013 Improving computational efficiency in global river models by implementing the local inertial flow equation and a vector-based river network map *Water Resour. Res.* **49** 7221–35
Yamazaki D, Kanae S, Kim H and Oki T 2011 A physically based description of floodplain inundation dynamics in a global river routing model *Water Resour. Res.* **47** 1–21
Yamazaki D, O'Loughlin F F E, Trigg M A, Miller Z F, Pavelsky T M and Bates P D 2014 Development of the global width database for large rivers *Water Resour. Res.* **50** 3467–80
Yang J, Yu L, Koblinsky C J and Adamec D 1998 Dynamics of the seasonal variations in the Indian Ocean from TOPEX/POSEIDON sea surface height and an ocean model *Geophys. Res. Lett.* **25** 1915–18
Zhao F et al 2017 The critical role of the routing scheme in simulating peak river discharge in global hydrological models *Environ. Res. Lett.* **12** 075003
Zheng F, Westra S, Leonard M and Sisson S A 2014 Modeling dependence between extreme rainfall and storm surge to estimate coastal flooding risk *Water Resour. Res.* **50** 2050–71
Zheng F, Westra S and Sisson S A 2013 Quantifying the dependence between extreme rainfall and storm surge in the coastal zone *J. Hydrol.* **505** 172–87
Zscheischler J et al 2018 Future climate risk from compound events *Nat. Clim. Chang.* **8** 469–77